

pubs.acs.org/acsapm Article

Extreme Plasticity, Adhesion, and Nanostructural Changes of Diblock Copolymer Microparticles in Cold Spray Additive Manufacturing

Ara Kim, Salih Duran, Apostolos Avgeropoulos, Sinan Müftü, and Jae-Hwang Lee*



Cite This: https://doi.org/10.1021/acsapm.3c01305



ACCESS

Metrics & More

Article Recommendations

Supporting Information

ABSTRACT: Using the laser-induced projectile impact testing (LIPIT), the extreme plastic and adhesive responses of polystyrene-polydimethylsiloxane block copolymer (BCP) microparticles are investigated to provide the ultra-high-strain-rate behavior of individual BCP feedstock powders during their collisions with a stationary substrate in the cold spray additive manufacturing process. The onset of BCP microparticle adhesion to the substrate is precisely predicted by the maximum coefficient of dynamic friction, quantified from the angled collisions, and by the spectra of the coefficients of restitution. This finding confirms the direct correlation between friction and adhesion mechanisms in the ultra-high-strain rate regime and its significance in the consolidation process of BCP feedstock powders. Furthermore, the impact-induced adiabatic shear flows create structural ordering of initially disordered nanostructures of the block copolymers consisting of glassy and rubbery domains while generating a temperature rise beyond their glass transition temperatures. In addition to the conventional strain-hardening effect in homopolymers, nanoscale morphological ordering can provide another strain-hardening mechanism of BCP feedstock microparticles in the cold spray of additive manufacturing.

KEYWORDS: Ultra-high-rate mechanics, laser-induced projectile impact test, adiabatic dynamic nonlinearity, energy dissipation, collision-induced nanostructures, nanosecond tribology

1. INTRODUCTION

Materials under excessive stress suffer plastic deformation accompanying irreversible structural changes at nano- and microscales. As plastic deformation becomes more extreme in terms of strain and strain rate, the molecular randomness of the structural changes increases, and the temperature of the material rises nonlinearly. Under such circumstances, low thermal diffusivity materials are expected to experience highly adiabatic and spatially localized thermal processes. Therefore, polymers' extremely rapid plastic deformations are intricate, since the temperature-dependent rheological properties incur complex interactions that change the mechanical properties. An additive manufacturing method, cold spray (CS), is recently being highlighted, as it can realize solid-state and solvent-free consolidation via high-velocity collisions (300–1200 m/s) of feedstock powders or ductile microparticles

 (μPs) for coating of polymers.⁵ However, the CS of polymers requires more extensive insights into the dynamic plasticity and interfacial response of polymers during the consolidation process.^{6–8} Because the collisions of high-velocity individual μPs last less than 1 μs , ⁹ the temperature profile inside each μP will have an exceptional gradient within the 1 μs length scale due to the polymer's low thermal diffusivity. ¹⁰ Thus, understanding the extreme plastic response of polymers under an ultra-high-rate (UHR) regime is crucial for rate-

Received: June 16, 2023 Accepted: August 10, 2023



and temperature-dependent material properties inducing brittle-to-ductile failure-mode transitions during the UHR collisions. ^{11,12} Moreover, gaining an adequate understanding of the UHR plasticity of polymers is essential for the applications of polymers expanding in defense and automotive fields, among others. ^{13,14}

Laser-induced projectile impact testing (LIPIT) has been recognized as one of the most effective methods to explore the extreme dynamic behavior of materials during UHR collision and is used for diverse collision-based research topics. 15,16 In particular, the deposition response of functional polymeric projectiles for CS was investigated to explore the critical impact velocity (v_c) for adhesion, which is determined by the material composition of the μ Ps and the substrates. ¹⁷ The molecularweight-dependent mechanical and rheological behavior of polystyrene µPs and substrates were also explored through LIPIT, and the results showed the collision-induced plastic shear flow and thermal softening resulting from viscoplastic work.¹⁸ However, the UHR plastic response, the resultant interfacial rheological characteristics, and the irreversibly produced nanostructural changes of polymeric µPs have not been sufficiently understood, and the material diversity is limited to homopolymers. The rate-dependent mechanical and temperature-dependent rheological properties causing the collision-induced extreme plastic behavior and morphologies are determined by the composition of the monomers and the configurations of their domains, such as their molecular weight, entanglement density, and nanostructure. 19,20 In particular, block copolymers (BCPs) consisting of multidomains with mechanically distinctive material properties are intriguing, as the rate- and temperature-dependent properties can be optimized for polymeric armor materials 15 and CS feedstock powders²¹ by tailoring the nanostructures. Collision-induced nanostructural changes, such as kink bands, segmental mixing, and orientation-dependent characteristics, were demonstrated via the supersonic collision of silica microspheres onto longrange-ordered BCP structures in the first LIPIT study. 15 The interfacial interactions between polymeric μPs and rigid ceramic substrates were systematically studied through LIPIT, and the results explained the extreme rate-dependent rheological response during collision.²² In a recent study, the characteristic energy dissipation mechanisms of both glassy and rubbery domains of BCP μ Ps, such as viscoplastic shear, tensile delamination, and frictional deposition under UHR conditions, were investigated with varying collision angles.² However, previous research did not directly connect the interfacial physics and the applicability of BCPs in CS by exploring the extreme plastic characteristics, interfacial response, and adhesion.

In order to understand the extremely dynamic and morphological response of polymer μ Ps, the μ Ps were fabricated by an ultrasonic atomization process and tested via the *advanced laser-induced projectile impact testing* (α -LIPIT)^{15,24} with a perpendicular collision angle onto stationary rigid silicon substrates to simplify complex collision physics by excluding viscoplastic deformation on the target side. Furthermore, because silicon's mechanical and thermal properties are well-known, the numerical modeling of collision physics can be more accurate. Compared to the experiment using actual CS equipment, α -LIPIT allowed us to investigate the dynamic behavior of BCP feedstock μ Ps at the single particle level. Although particles' collisions against the predeposited polymer particles are also essential in under-

standing the consolidation mechanisms of real cold spray, the findings from the simplified collision study utilizing LIPIT will still help us understand more complex dynamics between a particle and predeposited particles.

In addition, the effective coefficients of dynamic friction of the BCP and PS μ Ps, measured via 45° collisions, ²² were used to explore the relationship between the interfacial response and the critical velocity (ν_c) for adhesion. Moreover, the collision-induced morphological changes of the polymer nanostructures were investigated by comparing the nanostructural variations during collision using a 2D fast Fourier transform (2D FFT). The experimental data were used to develop a continuum model for finite element analysis and to estimate thermal and material parameters for the BCPs during the collision. A collision-induced nanostructural reordering in this study predicts that CS can be an additive manufacturing method enabling nanoscale-engineered materials through the extreme plastic deformation of the feedstock powers.

2. MATERIALS AND METHODS

2.1. Preparation and Characteristics of Polymer μ Ps. The model materials used in this research were polystyrene homopolymer (denoted as PS84) and two polystyrene-block-polydimethylsiloxane (PS-b-PDMS) BCPs (denoted as PS87-PDMS40 and PS83-PDMS83). The numbers of the designated polymer labels indicate the number-average molecular weight (M_n) of each polymer in kg· mol⁻¹. For example, PS87-PDMS40 is a BCP with PS of 87 in kg· mol⁻¹ and PDMS of 40 kg·mol⁻¹. The three polymers and their respective PS and PDMS blocks were sufficiently large in terms of $M_{\rm p}$ to expect an entanglement effect. Moreover, by selecting an M_n of PS that is nearly the same for all three polymers, the dynamic responses could be evaluated as a function of the volume fraction of the PDMS domain. Spherical polymer µPs were produced using ultrasonic atomization of a polymer solution with a weight ratio of 1:10 (polymer:toluene). The collected μ Ps were placed in a lab fume hood for at least 24 to eliminate residual solvent, and μ Ps' diameters were within a range between 10 and 30 μ m ($D_{50} = 16.8 \mu$ m). A more detailed experimental setup and procedure are described in Figure S1. The BCP µPs underwent microphase separations, yielding characteristic nanostructures during solvent evaporation due to the covalently bonded immiscible PS and PDMS chains. The morphologies of the nanostructures were randomly oriented with short-range ordering due to the high molecular weights 26 and fast fabrication time, regardless of particle sizes.²⁷ The volume fractions of glassy (f_{PS}) and rubbery $(f_{\rm PDMS})$ domains determined the nanostructures of the $\mu \rm Ps$ with cylindrical ($f_{\rm PDMS}$ ~ 30%) and lamellar ($f_{\rm PDMS}$ ~ 50%) morphologies,²⁸ as shown in the scanning electron microscopic (SEM) images of BCP μ Ps, cross-sectioned by focused ion beam milling (FIB) (Figure 1a,c). The randomly oriented phase-separated nanostructures were assumed to generate isotropic material characteristics of the μ Ps, confirmed by 2D FFT of the SEM images in Figure 1b,d. The near-circular pattern in 2D FFT indicated the isotropic nature of the structure and the existence of characteristic length scales of approximately 50 nm, corresponding to the average distance between cylinders or lamellae.

2.2. Microscopic Collision Experiment. During the performance of the α -LIPIT (Figure 2a), a single Nd:YAG laser pulse ablated a thin gold layer within a launching pad, and a μ P on it was accelerated toward a stationary substrate by the rapid inflation of an elastomer film (PDMS) of the launching pad. The UHR kinetic parameters of the polymer μ Ps during supersonic collisions were calculated with the inter- μ P distance in an ultrafast stroboscopic image (Figure 2b) and a designated time lag (Δt) of the α -LIPIT. As the entire trajectory of a μ P was recorded in a single image during impact, the UHR dynamic response from the image was used not only for kinetic parameters but also for the real-time deformation analysis of a μ P during impact.

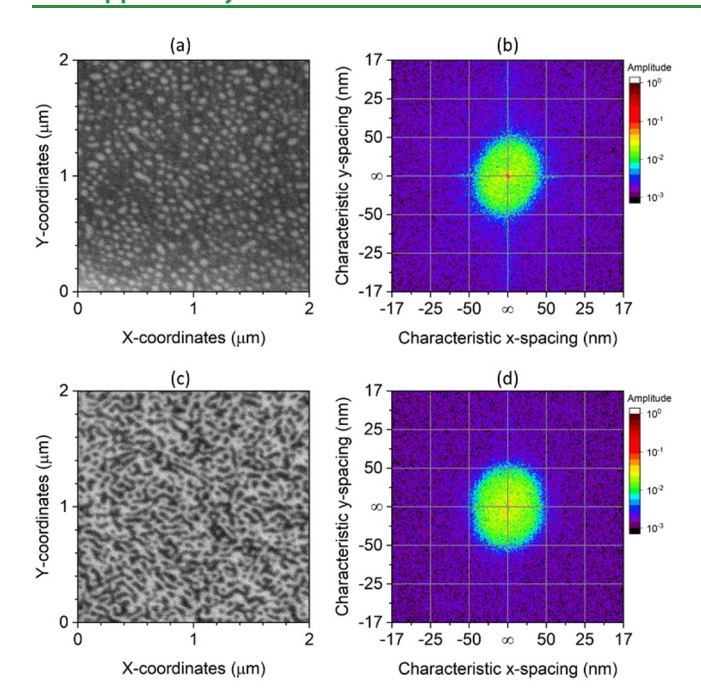


Figure 1. Structural characteristics of produced BCP μPs. (a) Cross-sectional SEM image and (b) FFT image of a PS87-PDMS40. (c) Cross-sectional SEM image and (d) FFT image of a PS83-PDMS83.

3. RESULTS AND DISCUSSION

3.1. Collision Kinetics and Adhesion. The range of the μ P's impact velocity (ν_i) , in which the polymer μ Ps adhere to the substrate, is defined as the adhesion window (AW) as shown in Figure 3. As the results do not present particle-size dependency within the size range which was used in this study, the figures are not visualized based on the particle sizes. The target substrates were silicon wafers (P-type) with thermal conductivity of 159 W·m⁻¹·°C⁻¹.²⁹ The substrates were considered rigid surfaces, and no signs of damage on the substrates were observed. The AW is one of the most

important indicators to determine whether a material is capable of the CS method,³⁰ since v_i out of this range will result in a significantly lower deposition efficiency. Typically, the lowest v_i value within the AW is v_c . Moreover, a broad AW is advantageous for higher deposition efficiency and flexible spray conditions. The AW of PS84 started at 594 m/s, while that of PS87-PDMS40 shifted to a significantly lower range (400-587 m/s). PS83-PDMS83 having a higher f_{PDMS} and total M_n than PS87-PDMS40 showed an AW at the lowest range of v_i . The AW of PS84 is expected to have an upper limit higher than the velocity range tested in this study, and an enormous thermal effect from plastic work is anticipated at the upper limit of the AW resulting in a partial-rubbery domain near the collision interface. The continuous morphology of the PS glassy domain of PS87-PDMS40 was supposed to limit shear motions of the PDMS rubbery domain, 23 and the resultant plastic deformations of μ Ps were also limited. In other words, the interconnected rubbery domain of PS83-PDMS83 allowed further plastic deformation and promoted adhesion.

3.2. Coefficient of Restitution. The dynamic behaviors of BCPs were analyzed with a quantitative framework using an empirical model for the coefficient of restitution (CoR), which is a ratio of the residual momentum of the BCP μ Ps. Since there was a negligible mass change of μP caused by the collision, CoR was simply defined by v_r/v_i . The collision response was assessed with the CoR spectra (Figure 4a-c), as they could convey the residual kinetic energy ratio before and after the collision of a μP impacting on a rigid substrate.³¹ Furthermore, the CoR spectra allowed indirect assessment of thermal softening resulting from extreme viscoplastic deformations. The CoR trends prior to reaching v_c were quantified by an empirical fitting model to explain the nonlinear inelastic characteristics by analyzing the material's plasticity and interfacial rate-dependent viscosity change. The UHR dynamic behavior of polymers is principally determined not only by the viscoplastic characteristics but also by the rate-dependent interfacial dynamic viscosity. Therefore, the exponential decay

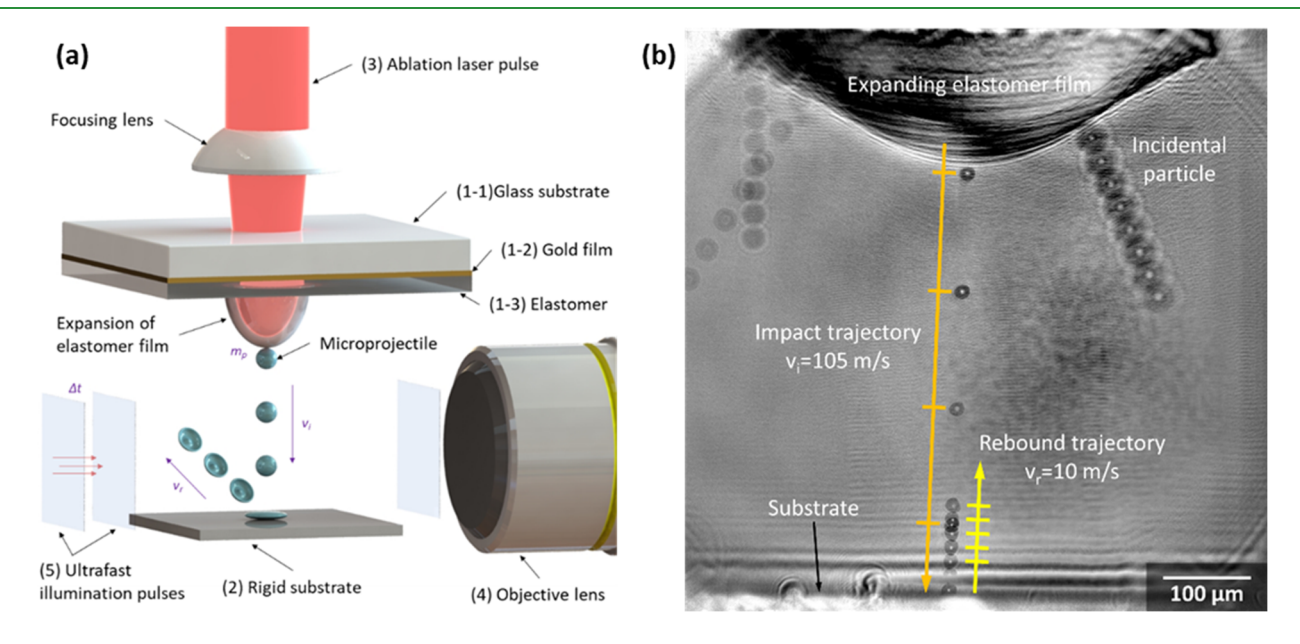


Figure 2. (a) Schematic of advanced laser-induced projectile impact test (α -LIPIT), and (b) ultrafast stroboscopic micrograph of α -LIPIT with motion indicators of a PS83-PDMS83 μ P during the entire collision process onto a silicon wafer substrate.

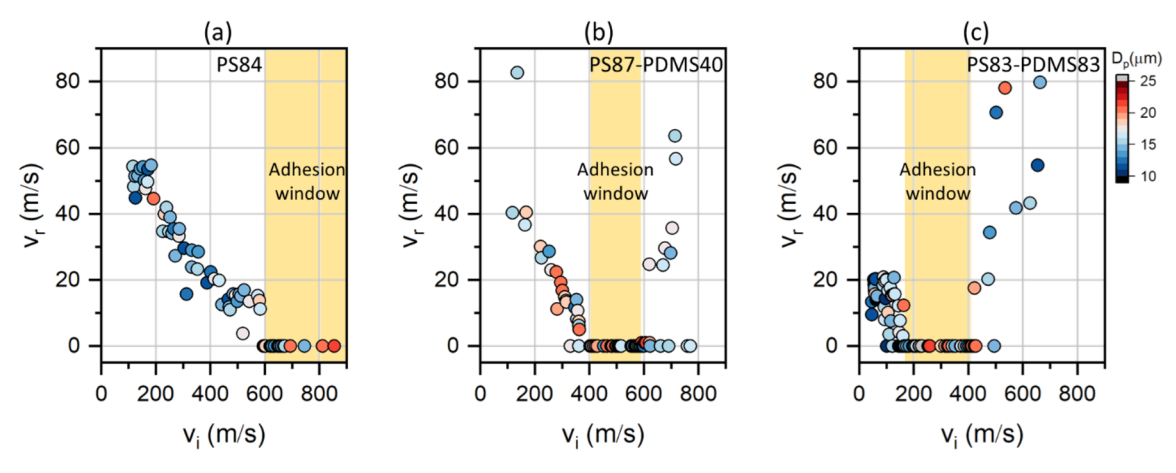


Figure 3. Dynamic and adhesive characteristics. ν_r spectra of (a) PS84, (b) PS87-PDMS40, and (c) PS83-PDMS83, where AWs are depicted as yellow regions.

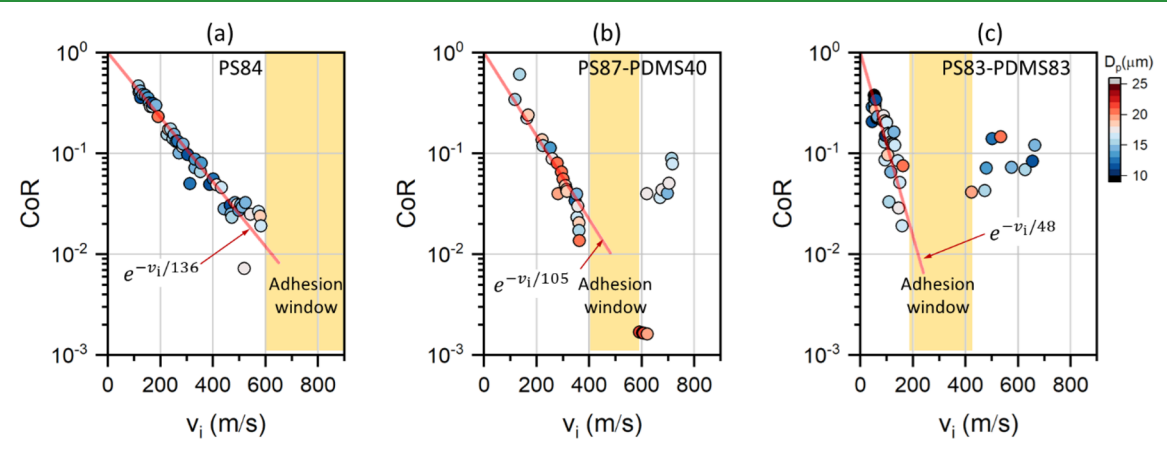


Figure 4. CoR spectra (dots) and the fitting curves (red lines) for (a) PS84, (b) PS87-PDMS40, and (c) PS83-PDMS83.

model physically originated from the Arrhenius equation, quantifying a degree of the dynamic thermal effects on polymers, including the impact-induced viscosity changes of a μP near the collision interface. This led to the exponentially decaying CoR model during collision onto a rigid substrate, which was also demonstrated in the previous LIPIT study: 18

$$CoR = \exp(-\nu_i/\alpha) \tag{1}$$

, where α is a single fitting parameter representing a characteristic velocity of the impact-induced thermal softening effect on the rheology of μ Ps during the collisions. This CoR model assumes that μP 's collision becomes entirely elastic as v_i approaches zero, which is suitable if μ P's interfacial adhesion with the substrate is negligible compared with μ P's volumetric viscoelastic response. Due to the technical difficulty in achieving v_i less than 100 m/s, the validity of this model was not confirmed for the low v_i regime, while this range is not very relevant for the typical CS process. The CoR fitting function only models the nonlinear plasticity when v_i is less than v_{ci} where a primary inelasticity is driven by volumetric shear deformation. The exponentially reduced inelasticity expressed by eq 1 suggests that the μ P's temperature was elevated with increasing v_{ij} creating a more adhesive force of μP on the substrate and overcoming the elastic recoiling when $v_i \ge v_c$. However, the existence of the upper bound of AW (especially in Figure 4b,c) implies that the actual process was nonmonotonic. One possible explanation is a transition from interfacial heating to volumetric heating, which will be discussed in the following section of the numerical simulations. When ν_i was higher than AW, fluctuating CoR behavior of BCP μPs was observed due to the two major instabilities, the interfacial shear instability 34 in the viscoplastic flows of μP and another instability in the separation of μP -substrate adhesive interfaces, influenced by the impact-induced thermal softening at the collision interface. 23 The decay parameter α for each polymer indicated that lower activation energy is required for the interfacial thermal effect inducing low dynamic viscosity as $f_{\rm PDMS}$ of a polymer increased. Note that although the upper limit of AW was not confirmed for PS84 in this study, we expect it can exist near 1000 m/s according to our recent study. 18

3.3. Numerically Modeled Temperature Profiles. The collision-induced localized thermal response of the μ Ps was computed through a continuum model using the commercially available finite element software package ABAQUS/Explicit version 2020 (Simulia, Pawtucket, RI, US) as shown in Figure 5. The simulations demonstrated that the maximum local temperature near the impact interface reached the glass-transition temperature of PS83-PDMS83 (103.6 °C; see SI for more experimental details) when $\nu_i > 300$ m/s. Furthermore, the maximum temperature zone near the periphery of the μ Ps indicated that the localized temperature increase resulted from the plastic shear flow propagating radially near the collision

ACS Applied Polymer Materials

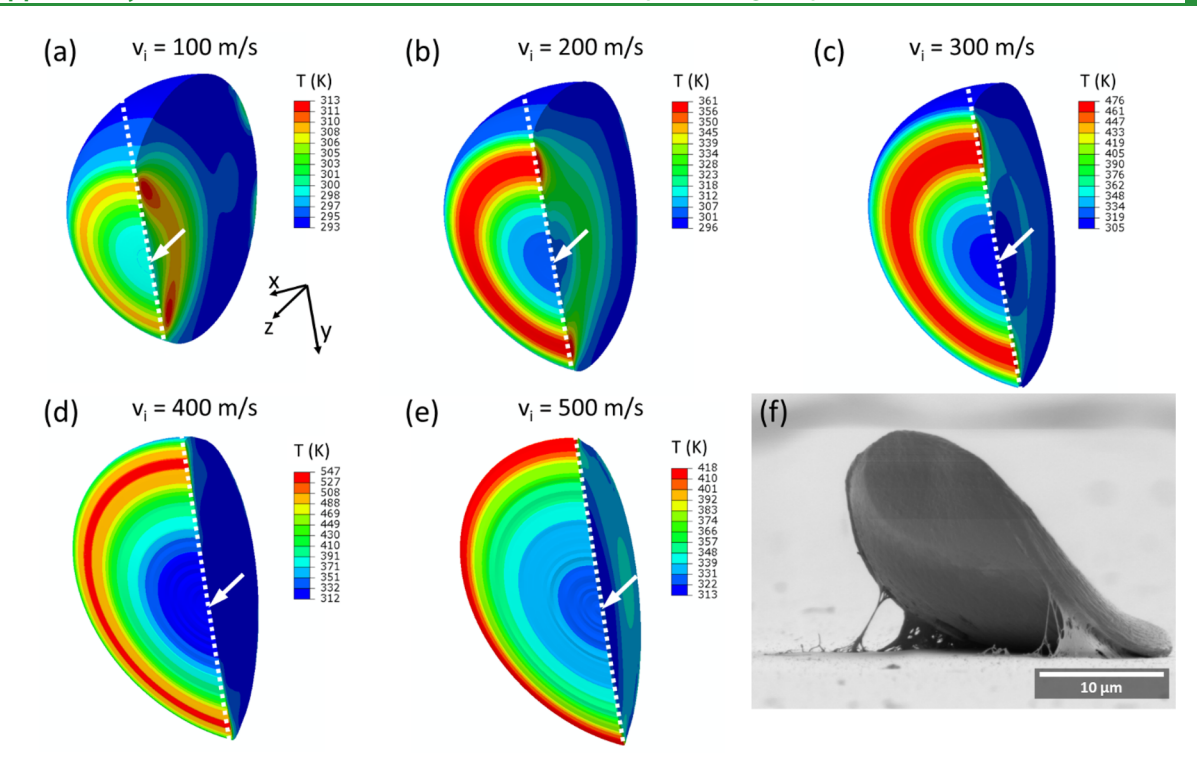


Figure 5. Computational simulation results show the temperature profiles at the impact face along the xy plane and the cross-sectional plane along the yz plane for (a) $v_i = 100$ m/s, (b) $v_i = 200$ m/s, (c) $v_i = 300$ m/s, (d) $v_i = 400$ m/s, and (e) $v_i = 500$ m/s when μ P's center of mass reaches zero. The white arrows and dashed lines indicate the impact direction along the z-direction and the surface of a substrate. (f) SEM image of a partially rebounded PS83-PDMS83 with $v_i = 451$ m/s exhibiting filaments at the periphery of the collision interface.

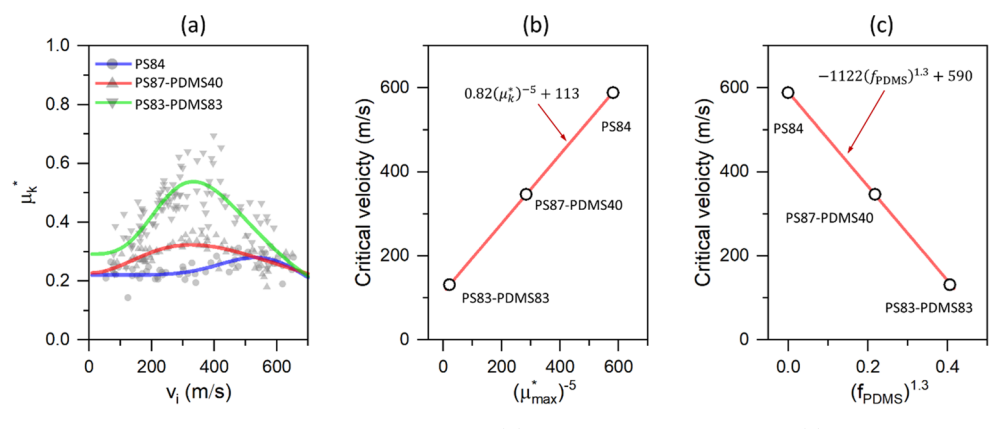


Figure 6. (a) Coefficients of dynamic friction reproduced from ref 22. (b) Correlation of v_c with μ_{max}^* (c) Correlation of v_c with f_{PDMS} .

interface during impact. The SEM image in Figure 5f qualitatively verified the simulation results. As the primary collision-induced deformation occurred in an extremely short duration (~20 ns), the increased chain mobility of the glassy domain was expected to be localized near the contact interface along the direction of propagation of the thermal effect without a phase transition. The model results supported the conclusion that the tribological response depends on collision-induced thermal softening and plastic flow near the collision interface. Interestingly, the maximum temperature at the adhesion interface was not monotonically increased but reduced at 500 m/s, while more heat was generated through the internal volume. This observation of more internal heat generation suggests that the μP became globally more flexible during its deformation and susceptible to localized bending (see Figures 5f and S4), reducing interfacial shear/heat. Consequently, the reduced interface temperature due to shifting the primary

energy dissipation region from the collision surface to the internal volume reduced the μ P's adhesion force and thus caused debonding/rebounding of a μ P at the upper limit of AW.

3.4. Tribological and Compositional Effects on Adhesion Threshold. The collision-induced coefficients of dynamic friction (μ_k^*) of PS and PS-b-PDMS were excerpted from ref 22, which were systemically investigated by performing 45° angled LIPIT experiments, and transformed into Figure 6a. In the 45° tilted collisions of μ Ps, two CoRs (CoRt and CoRn) along the normal and tangential directions were measured, and μ_k^* was calculated by $(\nu_{i,t}/\nu_{i,n})(1-\text{CoR}_t)/(1-\text{CoR}_n)$, where $\nu_{i,t}$ and $\nu_{i,n}$ are the tangential and normal components of μ P's initial velocity. We was used to demonstrate the interplay between μ_k^* and f_{PDMS} for adhesion. Higher f_{PDMS} increased μ_k^* because the M_n -dependent entanglement effect 35,36 strengthened the interchain resistance

ACS Applied Polymer Materials

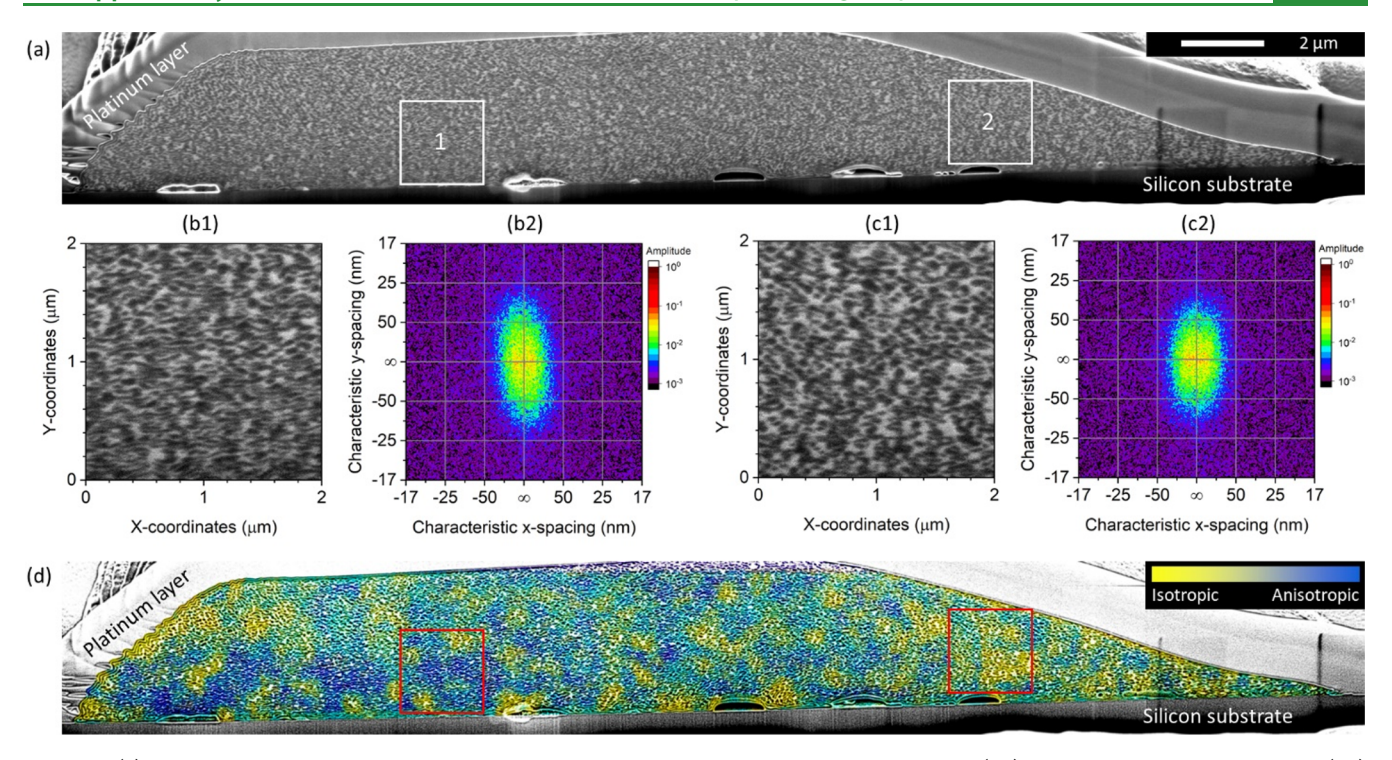


Figure 7. (a) Cross-sectional SEM image of a PS83-PDMS83 with $v_i = 586$ m/s and 2° incidence angle. (b1) Cross-sectional SEM image and (b2) FFT image of box 1 in (a). (c1) cross-sectional SEM image and (c2) FFT image of box 2 in (a). (d) Standard deviation map of domain isotropy.

during shear motion³⁷ along with the impact-induced rubbery transition of the PS chains near the collision interface. Although the number of entanglements per PS segment of all three samples is controlled around 6,⁴ the number of PDMS-segment increases from 0 (PS84), to 4 (PS87-PDMS40), to 8 (PS83-PDMS83).³⁸ Consequently, the rubbery-PDMS domain leads the μ Ps to adhere to the substrate by hindering the elasticity of the μ Ps and enhancing interfacial adhesion during the collision. The nonlinear correlations of ν_c with the maximum values of the μ_k^* spectra (Figure 6b) and with $f_{\rm PDMS}$ (Figure 6c) were expressed by the equations below:

$$v_{\rm c} \propto (\mu_{\rm max}^*)^{-5} \tag{2}$$

$$v_{\rm c} \propto (f_{\rm PDMS})^{1.3}$$
 (3)

As the correlation of adhesion-friction in soft materials has been investigated in a broad range of fields with fundamental questions,³⁹ eq 2 demonstrates the UHR correlation in the extreme circumstance between critical velocity for adhesion and the rheological responses of resulting in interfacial friction. Adhesion was not observed at the collision angle of 45°, and the collision-induced shear was anisotropic along the propagation direction of the μPs , which amplifies shearinduced interfacial responses. 22 On the contrary, radialdirectional shear was generated during the perpendicular collisions by compression stress flow within a limited interface, especially near the periphery of a μP with maximized thermal responses. Nonetheless, it is notable that the shear-induced rheological changes that were investigated at the angled LIPIT results can explain the adhesion onset condition, v_c at the perpendicular collision. In the application aspect, eq 3 is beneficial because it implies that AW can effectively be engineered by altering a rubbery portion of the BCP polymers.

3.5. Shear-Induced Nanostructural Ordering. As revealed in Figure 1, the BCP μ Ps were fabricated with short-range ordered nanostructures distinguishable from amorphous polymers like PS84. Due to the mechanical heterogeneity, postimpact nanostructures of bonded μP were investigated by the 2D FFT of the cross-sectioned images after FIB milling, as shown in Figure 7a. The impact-induced plastic deformations of a PS83-PDMS83 μ P were observed using high-resolution SEM and image processing. The FIB milling was conducted after the formation of a platinum or carbon protective layer via an electron beam (1 keV, 0.27 nA) and an ion beam (30 keV, 7.7 pA). The postimpact nanostructures presented significantly compressed and quenched interlamellar spacing (Figure 7b,c), compared to the isotropic nanostructures before impact shown in Figure 1. Due to the excessive flow stress resulting in inter-brush slip²³ followed by a rapid temperature rise during the short deformation time (<20 ns), segmental realignment occurred locally without the phase transition of the entire μP . This effect is accentuated further as the domain spacing becomes narrower near the collision interface, and the characteristic length scale decreases nearly 50% (25 nm) along the vertical direction to the contact surface, as shown in Figure 7d. This extensively compressed and horizontally ordered regions were produced by horizontal shear flows during the overall compressive deformation.

Furthermore, the mechanical properties of the ordered BCP, created by compressive shear flows, must be modified from the original ones; ^{40,41} one can expect *in situ* nanomechanical strengthening during the CS process.

4. CONCLUSIONS

In this study, the extreme plastic and adhesive response of BCP μ Ps with the $f_{\rm PDMS}$ -dependent configurations of domains are explored under the UHR collision conditions via LIPIT. The rubbery-PDMS domain of BCPs with high chain mobility

promotes plastic deformations and enhances the tribological response at the collision interface, which is preferable for adhesion during extreme plastic deformation. Furthermore, the interfacial thermal conditions and the rate-dependent rheological change resulting from the localized adiabatic shear softening near the collision interface determine the UHR dynamic behavior of BCPs. The collision-induced localized thermal effect increases the interfacial instability, weakening adhesion and incurring unsteady rebounding due to the temperature-dependent rheological changes near the collision interface. A sufficient volume fraction of the rubbery domain and the resultant effective coefficient of friction at the collision interface are advantageous to achieve a favorable AW with a high deposition efficiency and a feasible v_c of BCP μ Ps. In addition, the empirical fitting model of the CoR grounded on the rate-dependent interfacial viscosity change suggests criteria for the dynamic rheological response of multidomain BCPs. Moreover, the quantifications of $\nu_{\rm c}$'s using $\mu_{\rm k}^*$ and $f_{\rm PDMS}$ are used and verified by predicting AWs of μ Ps. Therefore, the fitting parameters for the quantifications of CoR and v_c representing the UHR dynamic and interfacial responses of polymers are expected to be utilized to determine the applicability and compatibility of polymers for CS products.

ASSOCIATED CONTENT

Supporting Information

The Supporting Information is available free of charge at https://pubs.acs.org/doi/10.1021/acsapm.3c01305.

Detailed ultrasonic atomization method; size distribution of produced polymer microparticles; glass transition temperatures and DSC data; numerical modeling method; and SEM images of deformed microparticles after rebounding (PDF)

AUTHOR INFORMATION

Corresponding Author

Jae-Hwang Lee — Department of Mechanical and Industrial Engineering, University of Massachusetts, Amherst, Massachusetts 01003, United States; Materials Science and Engineering Graduate Program, University of Massachusetts, Amherst, Massachusetts 01003, United States; orcid.org/0000-0002-2546-1044; Email: leejh@umass.edu

Authors

Ara Kim – Department of Mechanical and Industrial Engineering, University of Massachusetts, Amherst, Massachusetts 01003, United States; orcid.org/0000-0002-5776-8921

Salih Duran – Department of Mechanical and Industrial Engineering, Northeastern University, Boston, Massachusetts 02139, United States

Apostolos Avgeropoulos – Department of Materials Science Engineering, University of Ioannina, Ioannina 45110, Greece; occid.org/0000-0002-6203-9942

Sinan Müftü — Department of Mechanical and Industrial Engineering, Northeastern University, Boston, Massachusetts 02139, United States

Complete contact information is available at: https://pubs.acs.org/10.1021/acsapm.3c01305

Notes

The authors declare no competing financial interest.

ACKNOWLEDGMENTS

This research was supported by the National Science Foundation under [Grant No. CMMI-1760924]. We would like to express our special thanks to Dr. Roger Ristau and the CAMMA facility at UConn's Tech Park for their help in imaging with a focused ion beam equipment.

REFERENCES

- (1) Meyers, M.; Chawla, K. Plastic Deformation of Polymers. In *Mechanical Behavior of Materials*, 2nd ed.; Cambridge University Press, 2009; pp 188–192.
- (2) Hillmansen, S.; Hobeika, S.; Haward, R. N.; Leevers, P. S. The Effect of Strain Rate, Temperature, and Molecular Mass on the Tensile Deformation of Polyethylene. *Polym. Eng. Sci.* **2000**, *40* (2), 481–489.
- (3) Siviour, C. R.; Jordan, J. L. High Strain Rate Mechanics of Polymers: A Review. J. Dyn. Behav. Mater. 2016, 2 (1), 15–32.
- (4) Sperling, L. H. Introduction to Physical Polymer Science, 4th ed.; John Wiley & Sons, 2005. DOI: 10.1002/0471757128.
- (5) Lock Sulen, W.; Ravi, K.; Bernard, C.; Ichikawa, Y.; Ogawa, K. Deposition Mechanism Analysis of Cold-Sprayed Fluoropolymer Coatings and Its Wettability Evaluation. *J. Therm. Spray Technol.* **2020**, 29 (7), 1643–1659.
- (6) Papyrin, A.; Kosarev, V.; Klinkov, S.; Alkhimov, A.; Fomin, V. M. *Cold Spray Technology*; Elsevier, 2007. DOI: 10.1016/B978-0-08-045155-8.X5000-5.
- (7) Lee, J.-H.; Hassani, M. Studies of Single-Particle Impact. *Advances in cold spray* **2023**, 135–148.
- (8) Assadi, H.; Gärtner, F.; Stoltenhoff, T.; Kreye, H. Bonding Mechanism in Cold Gas Spraying. *Acta Mater.* **2003**, *51* (15), 4379–4394.
- (9) Veysset, D.; Lee, J.-H.; Hassani, M.; Kooi, S. E.; Thomas, E. L.; Nelson, K. A. High-Velocity Micro-Projectile Impact Testing. *Appl. Phys. Rev.* **2021**, *8* (1), No. 011319.
- (10) Nunes Dos Santos, W.; Mummery, P.; Wallwork, A. Thermal Diffusivity of Polymers by the Laser Flash Technique. *Polym. Test.* **2005**, 24 (5), 628–634.
- (11) Ravi-Chandar, K. On the Failure Mode Transitions in Polycarbonate under Dynamic Mixed-Mode Loading. *Int. J. Solids Struct.* **1995**, 32 (6–7), 925–938.
- (12) Ravi-Chandar, K.; Lu, J.; Yang, B.; Zhu, Z. Failure Mode Transitions in Polymers under High Strain Rate Loading. *Int. J. Fract.* **2000**, *101* (1–2), 33–72.
- (13) Irissou, E.; Legoux, J. G.; Ryabinin, A. N.; Jodoin, B.; Moreau, C. Review on Cold Spray Process and Technology: Part I Intellectual Property. *J. Therm. Spray Technol.* **2008**, *17* (4), 495–516.
- (14) Pearnchob, N.; Bodmeier, R. Dry Polymer Powder Coating and Comparison with Conventional Liquid-Based Coatings for Eudragit® RS, Ethylcellulose and Shellac. *Eur. J. Pharm. Biopharm.* **2003**, *56* (3), 363–369.
- (15) Lee, J.-H.; Veysset, D.; Singer, J. P.; Retsch, M.; Saini, G.; Pezeril, T.; Nelson, K. A.; Thomas, E. L. High Strain Rate Deformation of Layered Nanocomposites. *Nat. Commun.* **2012**, *3*, 1164–1169.
- (16) Xie, W.; Alizadeh-Dehkharghani, A.; Chen, Q.; Champagne, V. K.; Wang, X.; Nardi, A. T.; Kooi, S.; Müftü, S.; Lee, J.-H. Dynamics and Extreme Plasticity of Metallic Microparticles in Supersonic Collisions. *Sci. Rep.* **2017**, *7* (1), 5073.
- (17) Huang, M.; Liu, Y.; Khalkhali, Z.; Kim, A.; Hu, W.; Lee, J.-H.; Rothstein, J. P.; Klier, J.; Schiffman, J. D. Epoxy Resin-Encapsulated Polymer Microparticles for Room-Temperature Cold Sprayable Coatings. ACS Appl. Mater. Interfaces 2021, 13 (42), 50358–50367.
- (18) Gangineri Padmanaban, A.; Bacha, T. W.; Muthulingam, J.; Haas, F. M.; Stanzione, J. F.; Koohbor, B.; Lee, J.-H. Molecular-Weight-Dependent Interplay of Brittle-to-Ductile Transition in High-Strain-Rate Cold Spray Deposition of Glassy Polymers. *ACS Omega* 2022, 7 (30), 26465–26472.

- (19) Shaw, M. T.; MacKnight, W. J. Introduction to Polymer Viscoelasticity, 3rd ed.; John Wiley & Sons, 2005. DOI: 10.1002/0471741833.
- (20) Bukowski, C.; Zhang, T.; Riggleman, R. A.; Crosby, A. J. Load-Bearing Entanglements in Polymer Glasses. *Sci. Adv.* **2021**, 7 (38), 9763–9780.
- (21) Pracella, M. Micro- and Nanostructured Multiphase Polymer Blend Systems: Phase Morphology and Interfaces. *Macromol. Chem. Phys.* **2007**, 208 (2), 233.
- (22) Kim, A.; Müftü, S.; Thomas, E. L.; Lee, J.-H. Extreme Tribological Characteristics of Copolymers Induced by Dynamic Rheological Instability. ACS Appl. Polym. Mater. 2021, 3 (9), 4413–4418
- (23) Shan, W.; Weisbord, I.; Feng, X.; Hyon, J.; Manesi, G. M.; Avgeropoulos, A.; Segal-Peretz, T.; Thomas, E. L. Layered Thin Film Deposition via Extreme Inter-Brush Slip in a Lamellar Block Copolymer. *Macromolecules* **2022**, *55* (20), 9022–9029.
- (24) Lee, J.-H.; Loya, P. E.; Lou, J.; Thomas, E. L. Dynamic Mechanical Behavior of Multilayer Graphene via Supersonic Projectile Penetration. *Science* **2014**, 346 (6213), 1092–1096.
- (25) Panagiotou, T.; Levendis, Y. A. Generation of Spherical and Monodisperse Particles of Poly(Styrene) and Poly(Methyl Methacrylate) by Atomization of Monomers and Dissolved Polymer Precursors. J. Appl. Polym. Sci. 1991, 43 (8), 1549–1558.
- (26) Politakos, N.; Ntoukas, E.; Avgeropoulos, A.; Krikorian, V.; Pate, B. D.; Thomas, E. L.; Hill, R. M. Strongly Segregated Cubic Microdomain Morphology Consistent with the Double Gyroid Phase in High Molecular Weight Diblock Copolymers of Polystyrene and Poly(Dimethylsiloxane). *J. Polym. Sci., Part B: Polym. Phys.* **2009**, 47 (23), 2419–2427.
- (27) Yoshioka, A.; Tashiro, K. Solvent Effect on the Glass Transition Temperature of Syndiotactic Polystyrene Viewed from Time-Resolved Measurements of Infrared Spectra at the Various Temperatures and Its Simulation by Molecular Dynamics Calculation. *Macromolecules* **2004**, *37* (2), 467–472.
- (28) Bates, F. S. Polymer-Polymer Phase Behavior. *Science* **1991**, *251* (4996), 898–905.
- (29) University Wafer. https://www.universitywafer.com/silicon-wafer-application.html.
- (30) Grujicic, M.; Zhao, C. L.; DeRosset, W. S.; Helfritch, D. Adiabatic Shear Instability Based Mechanism for Particles/Substrate Bonding in the Cold-Gas Dynamic-Spray Process. *Mater. Des.* **2004**, 25 (8), 681–688.
- (31) Tillett, J. P. A. A Study of the Impact of Spheres on Plates. *Proc. Phys. Soc. Sect. B* **1954**, *67* (10), 794–805.
- (32) Lewandowska, K.; Dabrowska, A.; Kaczmarek, H. Rheological Properties of Pectin, Poly(Vinyl Alcohol) and Their Blends in Aqueous Solutions. *e-Polym.* **2012**, *12* (1), 15–27.
- (33) Stickel, F.; Fischer, E. W.; Richert, R. Dynamics of Glass-Forming Liquids. I. Temperature-Derivative Analysis of Dielectric Relaxation Data. *J. Chem. Phys.* **1995**, *102* (15), 6251–6257.
- (34) Fleck, N. A. Adiabatic Shear Instability: Theory. *Mechanical Properties and Testing of Polymers* **1999**, 3, 15–19.
- (35) Fetters, L. J.; Lohse, D. J.; Richter, D.; Witten, T. A.; Zirkel, A. Connection between Polymer Molecular Weight, Density, Chain Dimensions, and Melt Viscoelastic Properties. *Macromolecules* **1994**, 27 (17), 4639–4647.
- (36) Vorvolakos, K.; Chaudhury, M. K. The Effects of Molecular Weight and Temperature on the Kinetic Friction of Silicone Rubbers. *Langmuir* **2003**, *19* (17), 6778–6787.
- (37) Raghava, R. S.; Smith, R. W. Adhesion through Molecular Entanglements in Polymer Interfaces. J. Polym. Sci., Part B: Polym. Phys. 1989, 27 (12), 2525–2551.
- (38) Cai, L. H.; Kodger, T. E.; Guerra, R. E.; Pegoraro, A. F.; Rubinstein, M.; Weitz, D. A. Soft Poly(Dimethylsiloxane) Elastomers from Architecture-Driven Entanglement Free Design. *Adv. Mater.* **2015**, *27* (35), 5132–5140.
- (39) Urbakh, M.; Klafter, J.; Gourdon, D.; Israelachvili, J. The Nonlinear Nature of Friction. *Nature* **2004**, 430, 525–528.

- (40) Ye, C.; Singh, G.; Wadley, M. L.; Karim, A.; Cavicchi, K. A.; Vogt, B. D. Anisotropic Mechanical Properties of Aligned Polystyrene-Block-Polydimethylsiloxane Thin Films. *Macromolecules* **2013**, *46* (21), 8608–8615.
- (41) Kannan, R. M.; Kornfield, J. A. Evolution of Microstructure and Viscoelasticity during Flow Alignment of a Lamellar Diblock Copolymer. *Macromolecules* **1994**, *27* (5), 1177–1186.